Available online at www.sciencedirect.com
ScienceDirect
Catalysis Today 130 (2008) 302–308
CATALYSIS TODAY
www.elsevier.com/locate/cattod

Effect of Zr-SBA-15 support on catalytic functionalities of Mo, CoMo, NiMo hydrotreating catalysts

Shelu Garg, Kapil Soni, G. Muthu Kumaran, Manoj Kumar, J.K. Gupta, L.D. Sharma, G. Murali Dhar *

Catalytic Conversion Processes Division, Indian Institute of Petroleum, Dehradun 248005, India

Available online 3 December 2007

Abstract

SBA-15 and ZrO_2 (10–50 wt.%) containing SBA-15 mesoporous materials were prepared by direct and post-synthesis methods. Characterization using low angle XRD, pore size distribution, CO_2 chemisorption indicate that hexagonal mesoporous structure is retained even after ZrO_2 addition (25 wt.%). Mo, CoMo and NiMo catalysts prepared using these supports were examined by XRD, oxygen chemisorption, temperature programmed reduction (TPR). The catalysts were tested for hydrodesulfurization (HDS) of thiophene and hydrogenation (HYD) of cyclohexene. HDS of thiophene for 8%Mo, 3%Co8%Mo, and 3%Ni8%Mo increases with increasing ZrO_2 loading in SBA-15 up to 25 wt.%. Oxygen chemisorption and TPR hydrogen consumption indicated that the molybdenum dispersion and anion vacancies, and catalytic activities are significantly influenced by ZrO_2 content in Zr-SBA-15. A comparison indicated that TiO_2-SBA-15, ZrO_2-SBA-15 supported CoMo catalysts show higher activities for hydrodesulfurization.

Keywords: Mesoporous materials; SBA-15; ZrO_2-SBA-15; TiO_2-SBA-15; Hydrodesulfurization; Hydrogenation

1. Introduction

New generation hydrodesulfurization (HDS) catalysts are a necessity due to increasing stringent regulations on various petroleum products worldwide. For preparing hydrocarbon fuel feeds to the fuel cell set up requires sulfur reduction to near 0 ppm [1]. Many approaches have been pursued to achieve this challenging task, among which the variation of support is an important one [2–4]. γ-Al_2O_3 supported CoMo or NiMo catalysts have been widely studied. Many other supports like TiO_2 [5,6], ZrO_2 [7–10], SiO_2 [11], mixed oxides [12–14], Zeolites [15,16], and mesoporous materials [17–20] are also being studied for HDS with much interest. In several cases it is claimed that higher activities were obtained than those of commercial γ-Al_2O_3 supported catalysts [17–20]. The specific surface area of TiO_2 and ZrO_2 are very low and sensitive to temperature variation, however, their intrinsic activity for HDS is higher than γ-Al_2O_3 supported catalysts. Therefore, it is possible to prepare highly active HDS catalyst by increasing the surface area of TiO_2 and ZrO_2 support [21,22]. Ordered mesoporous silica (OMS) with high surface area and large pores makes an ideal candidate for preparing dispersed metals, pure and mixed metal oxides, sulfides, heteropoly-compounds by assembling them in the pore system of OMS. Many authors have studied the effect of preparation of catalyst materials by inserting Fe_2O_3 in MCM-41 [23], WS_2 [20], SO_4-ZrO_2 [24] and phosphotungstic acid [25] in SBA-15.

With the aim of increasing the surface area of ZrO_2 to use as a support for Mo catalysts, in this investigation, a systematic study was carried out on the variation of hydrotreating catalytic functionality with ZrO_2 loading over mesoporous silica SBA-15.

A comparison is made between ZrO_2 loaded SBA-15 catalysts with Zr incorporated SBA-15 supported catalysts.

To the best of our knowledge, this is the first time HDS catalysts are prepared using a support prepared by urea hydrolysis to obtain highly dispersed ZrO_2 nanoparticles inside the mesoporous SBA-15 materials.

* Corresponding author. Tel.: +91 135 2660146; fax: +91 135 2660202.
E-mail address: gmurli@iip.res.in (G.M. Dhar).

0920-5861/$ – see front matter © 2007 Elsevier B.V. All rights reserved.
doi:10.1016/j.cattod.2007.10.082

2. Experimental

2.1. Preparation of supports and catalysts

A series of ZrO_2-SBA-15 supports with varying ZrO_2 content (10–50 wt.%) was prepared by following post-synthetic homogeneous urea hydrolysis method. Hereafter, the above-prepared support would be denoted as Zr-SBA (P). SBA-15 mesoporous silica was prepared according to published procedure [26]. In a typical preparation of 10%Zr-SBA (P), 2.9055 g of Zirconium oxychloride ($ZrOCl_2{\cdot}8H_2O$, Aldrich) was mixed in 300 ml of water along with 2.7076 g of urea and dried SBA-15 (10 g). The mixture was stirred at 90 °C for 5 h. The obtained gel was filtered off, dried at 110 °C for 24 h followed by calcination in air at 550 °C for 6 h. Zirconium incorporated SBA-15 was prepared by direct synthesis method by following published procedure. The detailed procedure described elsewhere [27]. Hereafter, the above-prepared support would be denoted as Zr-SBA (D). For comparison purpose TiO_2 loaded SBA-15 was also prepared by following post-synthetic Impregnation–Evaporation (IE) method.

8%Mo, 3%Co8%Mo and 3%Ni8%Mo catalysts were prepared using the successive incipient-wetness impregnation method by taking corresponding nitrate salts on the above-prepared supports. The samples were dried at 120 °C for 24 h and calcined at 550 °C for 5 h.

2.2. Characterization

X-ray diffraction (XRD) patterns of the supports were recorded in the range $0.5 \leq 2\theta \leq 5$ and $10 \leq 2\theta \leq 90$ for supported catalysts in a D/max–2500 diffractometer using Cu Kα radiation (λ = 1.5418 Å). The specific surface area, pore volume and pore size distributions were measured by N_2 adsorption at −196 °C using Micromeritics ASAP 2010 (USA). The BJH method was applied to determine the pore size distribution. Temperature programmed reduction (TPR) was carried out on Micromeritics TPD/TPR 2900 instrument. Prior to TPR, the catalyst sample was preheated at 400 °C for 2 h in flowing He gas (ultra pure 99.99%). After the preheating, the carrier gas (5%H_2 in Ar, 50 ml/min) was purified by oxy trap and molecular sieves. The data were recorded while the temperature was ramped from ambient to 1000 °C at a heating rate of 10 °C/min. Low temperature oxygen chemisorption (LTOC) was carried out on both support as well as catalyst samples at −78°C (195 K) after sulfiding with CS_2/H_2 mixture at 400 °C followed by evacuation in a Pyrex glass static volumetric unit. The detailed procedure is described elsewhere [28]. CO_2 chemisorption of ZrO_2 containing supports and catalysts were carried out at 25 °C in order to evaluate the accessible zirconia surface area.

2.3. Catalytic activity

Catalytic activities were evaluated for HDS of thiophene and HYD of cyclohexene in a fixed bed catalytic micro-reactor operating at atmospheric pressure at 400 °C on presulfided catalyst using CS_2/H_2 mixture and interfaced with online gas chromatograph, the detailed procedure is described elsewhere [29].

3. Results and discussion

3.1. Low angle X-ray diffraction

SBA-15 with varying zirconia containing supports [Zr-SBA (P) and Zr-SBA (D)] are characterized by XRD and sorption techniques in order to establish the structural and textural properties. SBA-15 and Zr-SBA (P) samples show three diffraction peaks indexed as $d_{1\,0\,0}$, $d_{1\,1\,0}$, $d_{2\,0\,0}$ planes correspond to *p6mm* hexagonal symmetry. Fig. 1 shows the typical XRD pattern of pure siliceous SBA-15 and 25%Zr-SBA (P) samples. Both samples exhibit three diffraction peaks and the prominent peak due to $d_{1\,0\,0}$ planes has a *d*-value 110.3 Å. 25%Zr-SBA (P) shows similar pattern as SBA-15 indicating hexagonal order remains more or less intact after addition of ZrO_2. The peaks corresponding to $d_{1\,1\,0}$ and $d_{2\,0\,0}$ planes exhibit minor changes with ZrO_2 loading over SBA-15, revealing that there is slight structural modification of SBA-15 with ZrO_2 addition. Similar kind of diffraction pattern was obtained in all zirconia loaded samples (10, 35 and 50 wt.% ZrO_2). The XRD of Zr-SBA (D) also indicated low angle XRD peaks characteristic of hexagonal pore structure.

3.2. N_2 sorption analysis

All the SBA-15 supports with varying ZrO_2 content are examined by BET surface area and BJH pore size distribution. The N_2 adsorption–desorption isotherms of two typical samples [SBA-15 and 25%Zr-SBA (P)] are shown in Fig. 2. Both the

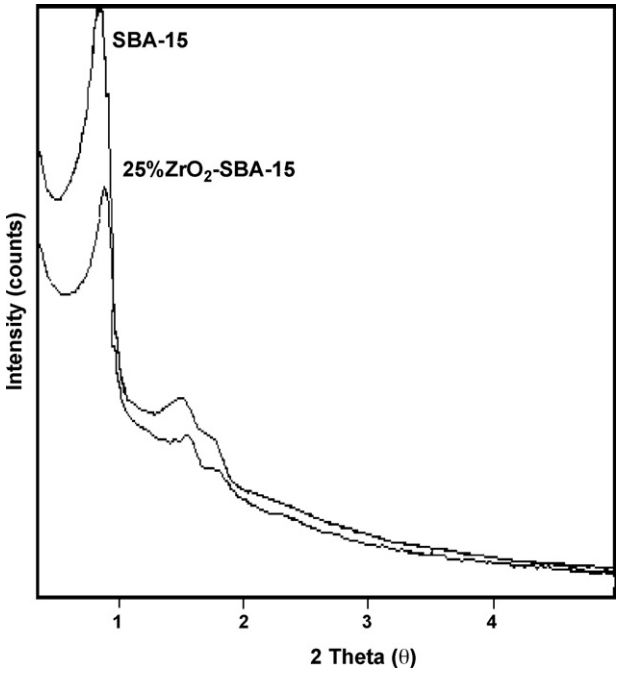

Fig. 1. Low angle XRD pattern of SBA-15 and 25%Zr-SBA (P) materials.

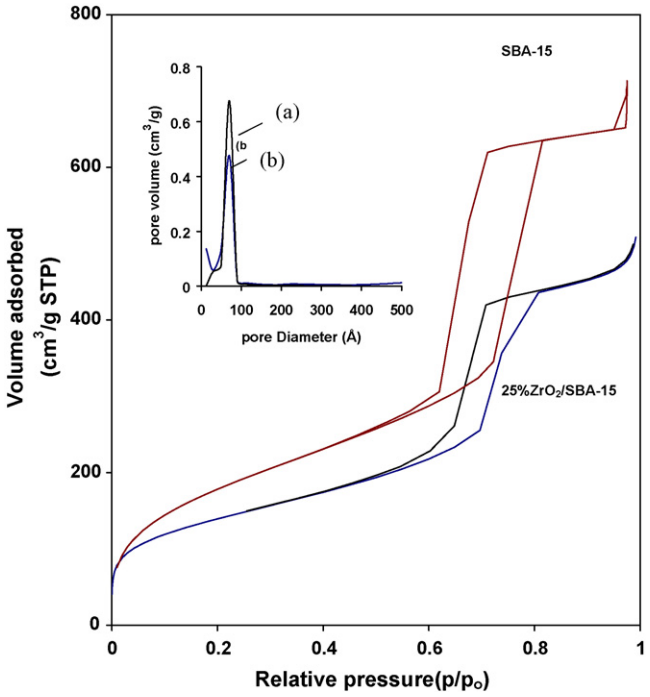

Fig. 2. N_2 adsorption–desorption isotherms and BJH pore size distribution (insert) of SBA-15 and 25%Zr-SBA (P) materials.

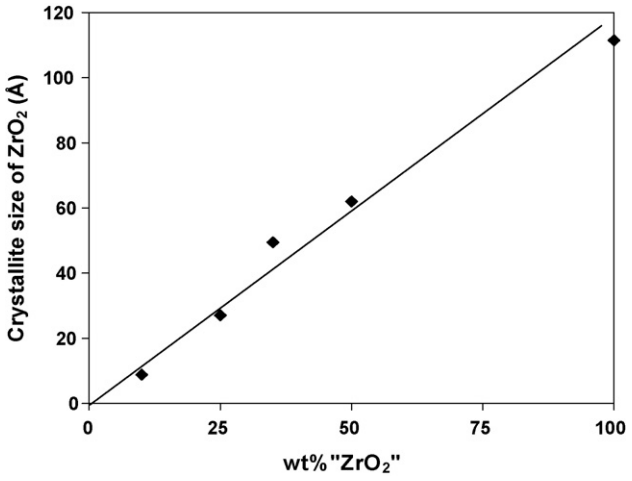

Fig. 3. Correlation of CO_2 uptake and crystallite size of ZrO_2 with wt.% of ZrO_2 in SBA-15.

samples exhibit typical type-IV isotherms with hysteresis loop, which correspond to hexagonal pore system. It can be seen that the height of hysteresis loop decreases with increasing ZrO_2 content showing that the mesopore-adsorbed volumes of gases decrease with ZrO_2 loading over SBA-15. The insert figure shows the narrow pore size distribution of SBA-15 as well as 25%Zr-SBA (P) samples centered on 66.3 and 65.9 Å, respectively. The details about the textural characterization of all the supports and catalysts are shown in Table 1. Mean pore size diameter (D_{BJH}) decrease with increasing ZrO_2 loading from 66.3 to 40.8 Å in SBA-15, the total pore volume (V_t) decreasing from 0.96 to 0.25 cm^3/g and the specific surface area (S_{BET}) from 717 to 317 m^2/g with ZrO_2 loading [Zr-SBA (P)], indicate that the zirconia is mainly located inside the SBA-15 mesoporous channel. Landau et al. [30,31] prepared ZrO_2 (48–75 wt.%) and TiO_2 (30–80 wt.%) nanocrystals inside the SBA-15 mesoporous channel by chemical solution deposition and internal hydrolysis methods and observed ink-bottle type pores for samples containing ZrO_2 and TiO_2 inside the SBA-15. They concluded that high ZrO_2 or TiO_2 loading leads to form larger nanocrystals, which have potential to block the pores of SBA-15.

Here, we used homogeneous urea hydrolysis method which results in highly dispersed zirconium oxide at lower ZrO_2 content. The ZrO_2 crystallite size seems to increase with increasing ZrO_2 loading over SBA-15 from 10 to 50 wt.%. This leads to the decrease of mean pore diameter as well as the total pore volume.

3.3. CO_2 chemisorption

CO_2 chemisorption is a useful technique to study the ZrO_2 dispersion [32,33]. CO_2 selectively chemisorbs on ZrO_2 allows us to measure the crystallite size in a similar manner to that of MoS_2 [28]. We evaluated the crystallite size of ZrO_2 and plotted against ZrO_2 wt.% over SBA-15 as shown in Fig. 3. It shows that ZrO_2 crystallite size increases with increasing ZrO_2 content in SBA-15. Therefore, the dispersion of ZrO_2 decreases with ZrO_2 content in the range 10–50 wt.% of ZrO_2.

From the above discussion, it is clear that we are dealing with mesoporous SBA-15 material where ZrO_2 is loaded inside the SBA-15 mesoporous channel in a highly dispersed state. Depending upon the loading of ZrO_2, the crystallite size of ZrO_2 varies inside the SBA-15 tubular channel. However, all the ZrO_2 loaded SBA-15 exhibit X-ray amorphous phase even at 50 wt.% ZrO_2 indicating that ZrO_2 is highly dispersed at all loadings. Similar characterization studies were performed on

Table 1
Textural characterization of Zr-SBA (P) supports with varying ZrO_2 content

Sample	D_{BJH} (Å)	V_t (cm^3/g)	S_{BET} (m^2/g)	S_{mic} (m^2/g)	S_{ex} (m^2/g)
SBA-15	66.3	0.96	717	141	576
25%Zr-SBA (P)	65.4	0.78	504	50	454
35%Zr-SBA (P)	48.3	0.45	375	0	375
50%Zr-SBA (P)	40.8	0.25	252	0	252
(20) Zr-SBA (D)	68.3	0.95	634	195	439
8%Mo25%Zr-SBA (P)	65.3	0.55	317	33	284

D_{BJH}: mean pore diameter; V_t: total pore volume; S_{BET}: total surface area; S_{mic}: micropore area; S_{ex}: external surface area.

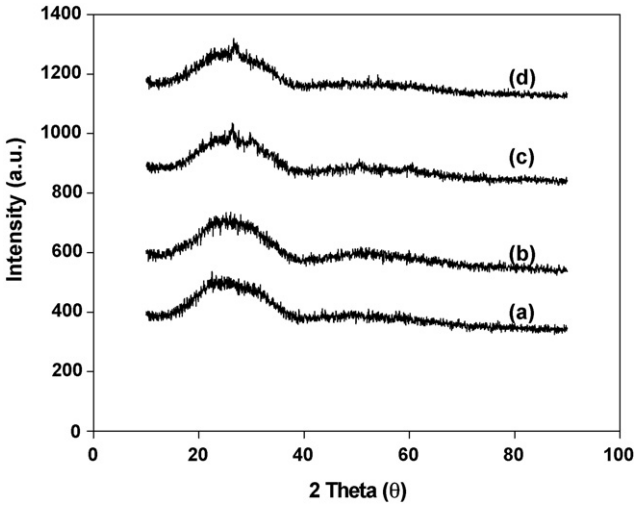

Fig. 4. XRD patterns of (a) 8%Mo-10%Zr-SBA-15 (P); (b) 8%Mo-25%Zr-SBA (P); (c) 8%Mo-35%Zr-SBA (P) and (d) 8%Mo-50%Zr-SBA (P).

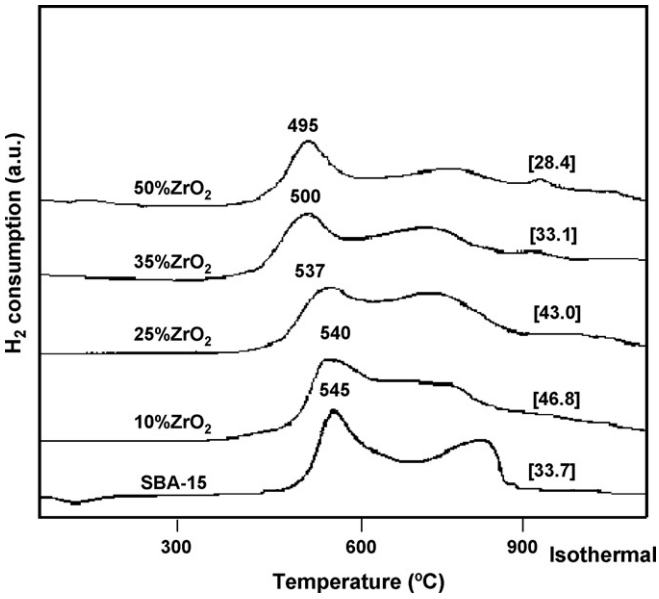

Fig. 5. TPR patterns of 8%Mo/(*x*)Zr-SBA (P) and SBA-15 supported catalysts (value in the parenthesis indicates H_2 consumption per gram of cat.).

Zr-SBA (D) samples which showed narrow pore size distribution similar to SBA-15 shown in Table 1. For comparison purpose 25%TiO_2-SBA-15 is also prepared and characterized in a similar way. TiO_2 forms a mixture of anatase and rutile phases at 25 wt.% over SBA-15 prepared following Impregnation–Evaporation method.

Powder XRD pattern for 8%Mo catalysts supported on Zr-SBA (P) materials are shown in Fig. 4. No XRD reflections were observed on 8%Mo-SBA-15 catalysts at various ZrO_2 content indicates that MoO_3 as well as ZrO_2 are well dispersed over SBA-15 and both ZrO_2 and MoO_3 show XRD amorphous phase indicating that the crystallite size less than 40 Å.

3.4. Temperature programmed reduction

The TPR results for 8%Mo/(*x*)Zr-SBA (P) catalysts are shown in Fig. 5 and for comparison purpose SBA-15 supported catalyst is also included. All the samples show the typical two peak reduction patterns corresponding to $Mo^{+6} \rightarrow Mo^{+4} \rightarrow Mo$ steps. The low temperature peak is associated with complete reduction ($Mo^{+6} \rightarrow Mo^{+4}$) of polymeric octahedral Mo species weakly bound to the support and the high temperature peak is associated with complete reduction (Mo^{4+} to Mo) of polymeric octahedral, tetrahedral and bulk crystalline MoO_3. As ZrO_2 content increases in SBA-15 the first primary reduction peak shifts towards lower side along with gradual increase of peak area. It shows that low temperature reducible species of Mo are preferentially forming over 10 and 25 wt.% ZrO_2 loaded SBA-15 supports. In contrast, very high ZrO_2 loaded [35%Zr-SBA (P) and 50%Zr-SBA (P)] samples exhibit relatively low amount of low temperature reducible species. The H_2 consumption per gram of support values in the TPR profile also support this conclusion that the reducibility of molybdenum increases with increasing zirconia loading and passes through a maximum (25 wt.%). It indicates that molybdenum is preferentially interacting with zirconia in preference to silicious portion in all the above-mentioned supports.

3.5. Catalytic activity

The catalytic activities were evaluated for HDS of thiophene and hydrogenation of cyclohexene as a function of ZrO_2 content and shown in Table 2. A typical result for HDS of thiophene on 8%Mo, 3%Co8%Mo, and 3%Ni8%Mo catalysts

Table 2
Catalytic activity for HDS of thiophene and HYD of cyclohexene on (*x*)Zr-SBA (P) supported 8%Mo, 3%Co8%Mo, and 3%Ni8%Mo catalysts

Sample	HDS rate[a] (mol h^{-1} g^{-1} × 10^{-3})			HYD rate (mol h^{-1} g^{-1} × 10^{-3})			Selectivity K_{HYD}/K_{HDS}		
	8%Mo	3%Co8%Mo	3%Ni8%Mo	8%Mo	3%Co8%Mo	3%Ni8%Mo	8%Mo	3%Co8%Mo	3%Ni8%Mo
SBA-15	24	49.1	39.6	25.7	41.2	32.5	1.07	0.84	0.82
10%Zr-SBA (P)	31.1(33)	53.2(47)	44.7(56)	10.5	22.6	33.2	0.33	0.42	0.74
25%Zr-SBA (P)	44.0(45)	72.3(80)	67.4(85)	18.8	23.4	48.3	0.43	0.32	0.71
35%Zr-SBA (P)	36.1(25)	43.7(36)	57.3(19)	19.4	15.2	29.7	0.54	0.34	0.79
50%Zr-SBA (P)	31.0(20)	30.0(35)	59.6(10)	20.6	15.9	24.1	0.66	0.53	0.40
(33)Zr-SBA (D)	51.0(56)	57.0(63)	65.0(60)	31.0	39.0	57.0	0.60	0.68	0.87
(20)ZR-SBA (D)	56.0(64)	69.0(69)	70.0(65)	34.0	50.0	72.0	0.60	0.72	1.02
ZrO_2	6.7	15.0	9.2	2.5	1.9	1.1	0.37	0.12	0.12

[a] The data in the parenthesis is O_2 uptake in μmol/g.

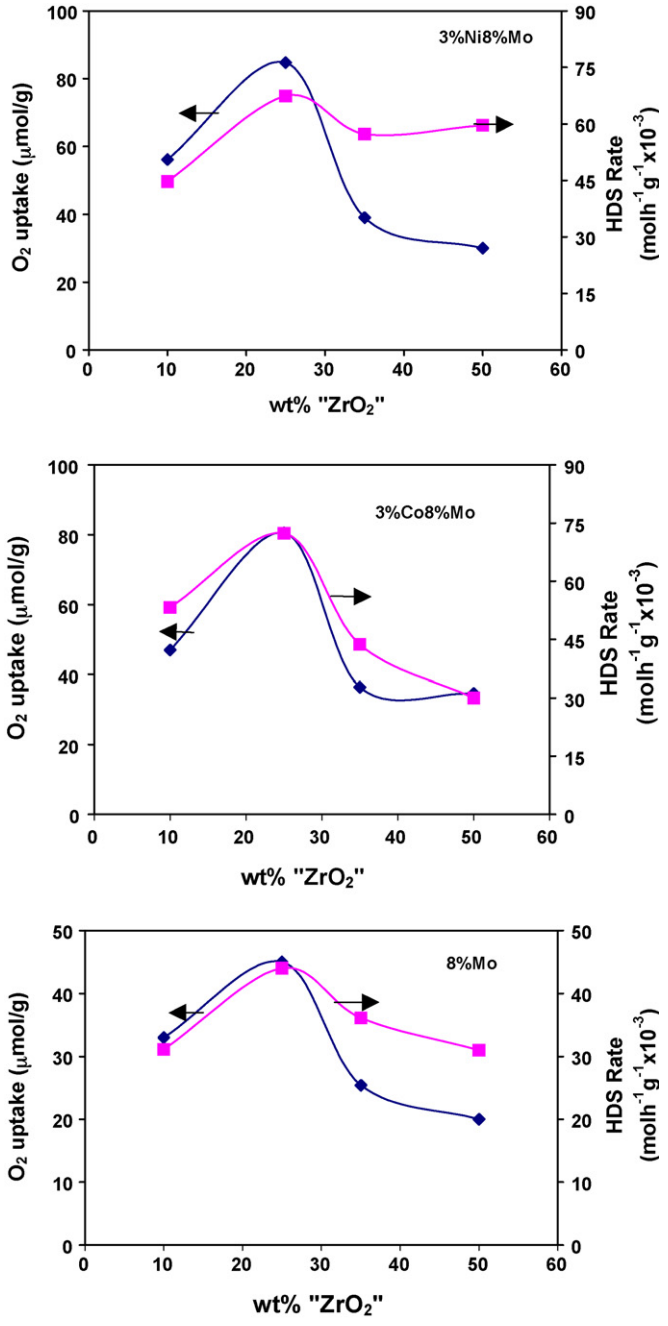

Fig. 6. Variation of O_2 uptake and thiophene HDS rate with ZrO_2 loading on Zr-SBA (P) supported catalysts.

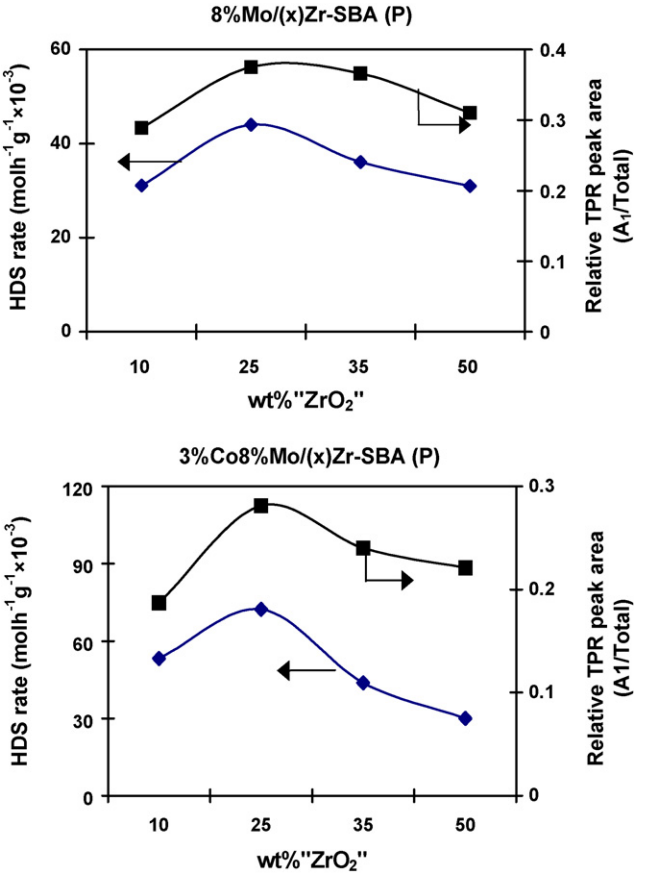

Fig. 7. Effect of HDS reaction rate and reducibility (A_1/total area) with ZrO_2 loading on 8%Mo and 3%Co8%Mo catalysts.

were plotted against ZrO_2 content in Zr-SBA (P) and shown in Fig. 6. It can be noted that the HDS rate increases with ZrO_2 content on Mo, CoMo, and NiMo catalysts up to 25 wt.% and beyond this it shows a decreasing trend. It can also be noted from Table 2 and Fig. 6 that there is significant promotional effect by Co and Ni for HDS reaction and there is no such clear trend in the case of hydrogenation. Similar results on HYD of TiO_2 and ZrO_2 supported Mo catalysts often also observed by many researchers [34,10]. Ni seems to have better hydrogenation activity than Co promoted catalysts on all the supports agreeing with the well-known fact on γ-Al_2O_3 supported catalysts.

It is interesting to see from Fig. 6 that O_2 uptake measured for assessing the dispersion of molybdenum follows the similar trend as activity. Oxygen chemisorbs on anion vacancies and represents number of vacancies in Mo and W systems [35]. It is well known that HDS reaction takes place on anion vacancies [36]. Both oxygen uptake as well as HDS activity show maxima at 25 wt.% ZrO_2 loading on Mo, CoMo, and NiMo catalysts indicating that highly dispersed catalysts of Mo and their promoted catalysts were obtained on 25%Zr-SBA (P) support.

Variation of HDS of thiophene on 8%Mo and 3%Co8%Mo supported over Zr-SBA (P) and the useful reducibility (relative TPR peak area) with ZrO_2 loading are shown in Fig. 7. Both HDS activity as well as relative TPR peak area is passing through a maximum at 25 wt.% ZrO_2. It shows that the low temperature reducible Mo species increase with ZrO_2 content up to 25 wt.% and drop at higher loading. It appears that the low temperature reducible species are mostly contributing to the observed HDS activity. This trend was also shown by 3%Co8%Mo promoted catalysts as seen in Fig. 7(b). Therefore, it appears that the molybdenum reducibility is the key factor in determining the activity of these catalysts. From the above discussion it is clear that dispersion as well as reducibility of Mo and CoMo catalysts increase with increasing ZrO_2 content in SBA-15 up to 25 wt.% and beyond this loading both parameters follow decreasing trend. HDS of thiophene also

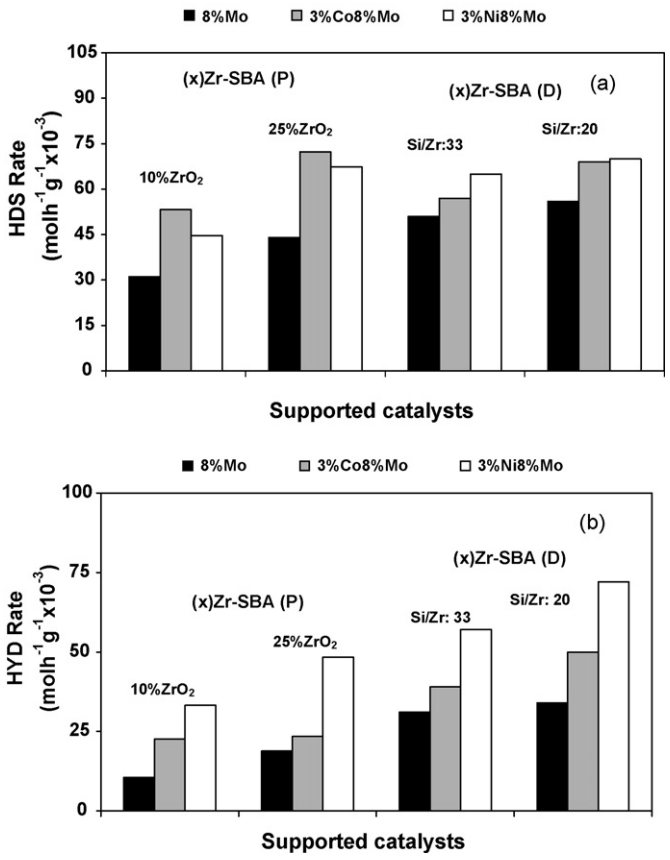

Fig. 8. Comparison of (a) HDS; (b) HYD activity of 8%Mo, 3%Co8%Mo and 3%Ni8%Mo catalysts supported on Zr-SBA (P) and Zr-SBA (D) materials.

shows similar behavior as the dispersion and reducibility as the function of ZrO_2 content.

In order to get insight into the effect of method of introduction of ZrO_2 on to SBA-15 on hydrotreating catalytic functionalities, a comparison has been made for HDS of Mo, CoMo and NiMo on Zr-SBA (P) (10 and 25 wt.%) with Zr-SBA-15 (D) (Si/Zr ratio 20 and 33) supported catalyst samples

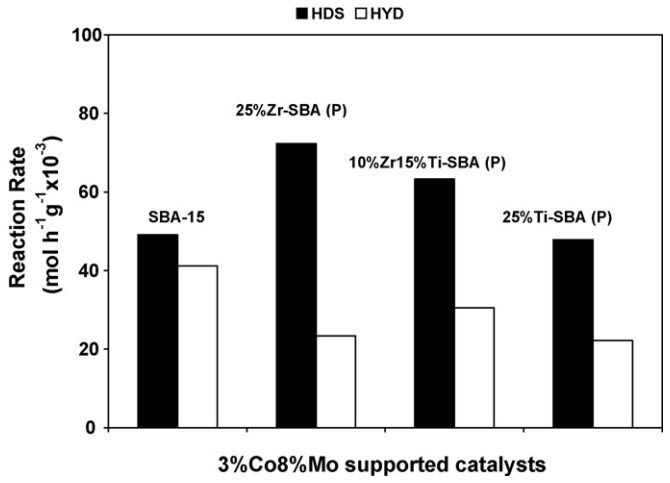

Fig. 9. Comparison of HDS and HYD activity of 3%Co8%Mo catalyst supported on 25%Zr-SBA (P), 10%Zr-15%Ti-SBA (P) and 25%Ti-SBA (P) materials.

(Fig. 8). It can be seen that Mo catalysts supported over Zr-SBA (D) show slightly higher HDS and hydrogenation activity than catalyst prepared from Zr-SBA (P) by post-synthesis method. In the case of promoted catalysts, both ZrO_2-SBA-15 supports yield more or less the same HDS activity. Co and Ni promoted catalysts on Zr-SBA-15 (D) gave almost two times higher HYD activity than on Zr-SBA (P) support. The reason for such an observation is not clear, further investigations are in progress to understand the phenomena.

A comparison of TiO_2-SBA-15 with ZrO_2-SBA-15 is made in Fig. 9. It can be seen that 25%Zr-SBA (P) shows highest activity for HDS reaction. However, hydrogenation activity is higher in the case of pure SBA-15 supported catalysts. Introduction of TiO_2 results in marginal increase in activity for HDS, however, HYD activity is lower in this case also. Introduction of TiO_2 on to ZrO_2-SBA-15 did not show any synergistic effect. This variation in HDS and HYD indeed indicate that the support independently varies the HDS and HYD catalytic functionalities.

4. Conclusions

SBA-15 mesoporous silica was effectively used for dispersing ZrO_2 and TiO_2 by direct as well as post-synthesis methods. These materials were used to prepare Mo, CoMo, and NiMo catalysts. Characterization of Zr-SBA (P) supports show that ZrO_2 is highly dispersed over SBA-15 up to 25 wt.% loading and their supported catalysts also exhibit the similar trend for dispersion of MoS_2. CO_2 chemisorption of Zr-SBA-15 (P) supports show that the crystallite size of ZrO_2 increases with ZrO_2 loading on SBA-15. XRD results on 8%Mo/(*x*)Zr-SBA (P) show that there is no evidence for presence of crystalline phases indicating both Mo as well as ZrO_2 are dispersed well on all the studied Zr-SBA-15 supports. Low temperature reducible molybdenum species are preferentially formed on low ZrO_2 content SBA-15 supports (10 and 25 wt.%). These low temperature reducible Mo and CoMo species exhibit a nice correlation with catalytic activity on ZrO_2 containing SBA-15 supports suggesting that the added ZrO_2 enhances the formation of low temperature reducible species which appears to be responsible for catalytic activity. Zr-SBA-15 supported molybdenum catalysts prepared by both direct and post-synthesis methods show more or less the same HDS activity but Zr-SBA (D) supported catalysts exhibit higher hydrogenation activity. The observed increase in hydrogenation activity may not be due to increase in molybdenum dispersion as can be seen from the oxygen uptake data in Table 2. It may be due to individual isolated Zr ions in the SBA-15 structure, affecting the properties of CoMo, NiMo catalysts in a different way. However, further studies are needed to support the hypothesis.

Acknowledgements

The authors are grateful to Director, Indian Institute of Petroleum, Dehradun for his encouragement and S. Garg, K. Soni, G.M. Kumaran thanks CSIR, India for providing fellowships.

References

[1] Fuel Processing for Fuel Cell applications, Special Issue of Catal. Today, in Saikatikaneni, A.M. Gaffrey, C. Song (Eds.), Catal. Today 77 (2002) and paper there in.

[2] Y. Okamoto, M. Breysse, G.M. Dhar, C. Song, Effect of support in hydrotreating catalysis for ultra clean fuels, Catal. Today 86 (1–4) (2003) (Special issue).

[3] G. Murali Dhar, B.N. Srinivas, M.S. Rana, M. Kumar, S.K. Maity, Catal. Today 86 (2003) 45.

[4] M. Breysse, P. Afanasiev, C. Geantet, M. Vrinat, Catal. Today 86 (2003) 5.

[5] L.C. Caero, A.R. Romero, J. Ramirez, Catal. Today 78 (1–4) (2003) 513.

[6] S.K. Maity, M.S. Rana, S.K. Bej, J. Ancheyta-Juárez, G. Murali Dhar, T.S.R. Prasada Rao, Appl. Catal. A: Gen. 205 (1–2) (2001) 215.

[7] M.C. Barrera, M. Viniegra, J. Escobar, M. Vrinat, J.A. de los Reyes, F. Murrieta, J. García, Catal. Today 98 (1–2) (2004) 131.

[8] P. Afanasiev, M. Cattenot, C. Geantet, N. Matsubayashi, K. Sato, S. Shimada, Appl. Catal. A: Gen. 237 (1–2) (2002) 227.

[9] S.K. Maity, M.S. Rana, B.N. Srinivas, S.K. Bej, G. Murali Dhar, T.S.R. Prasada Rao, J. Mol. Catal. A: Chem. 153 (1–2) (2000) 121.

[10] Y. Ji, P. Afanasiev, M. Vrinat, W. Li, C. Li, Appl. Catal. A: Gen. 257 (2004) 157.

[11] G. Murali Dhar, F.E. Massoth, J. Shabtai, J. Catal. 85 (1984) 44.

[12] S. Damyanova, L. Petrov, M.A. Centeno, P. Grange, Appl. Catal. A: Gen. 224 (1–2) (2002) 271.

[13] M.S. Rana, E.M.R. Capitaine, C. Leyva, J. Ancheyta, Fuel 86 (9) (2007) 1254.

[14] M.S. Rana, S.K. Maity, J. Ancheyta, G. Murali Dhar, T.S.R. Prasada Rao, Appl. Catal. A: Gen. 268 (1–2) (2004) 89.

[15] D. Li, A. Nishijima, D.E. Morris, J. Catal. 182 (2) (1999) 339.

[16] W.J.J. Welters, G. Vorbeck, H.W. Zandbergen, J.M. van de Ven, E.M. van Oers, J.W. de Haan, V.H.J. de Beer, R.A. van Santen, J. Catal. 161 (2) (1996) 819.

[17] A. Wang, Y. Wang, T. Kabe, Y. Chen, A. Ishihava, W. Qian, P. Yao, J. Catal. 210 (2002) 319.

[18] G.M. Kumaran, S. Garg, K. Soni, M. Kumar, L.D. Sharma, G. Murali Dhar, K.S. Rama Rao, Appl. Catal. A: Gen. 305 (2006) 123.

[19] T.A. Zepeda, T. Halachev, B. Pawelec, R. Nava, T. Klimova, G.A. Fuentes, J.L.G. Fierro, Catal. Commun. 7 (1) (2006) 33.

[20] L. Vradman, M.V. Landau, M. Merskowitz, V. Ezersky, M. Talianka, S. Nikitenko, Y. Koltypin, A. Gedanken, J. Catal. 213 (2003) 163.

[21] O.Y. Gutierrez, G.A. Fuentes, C. Salcedo, T. Klimova, Catal. Today 116 (2006) 485.

[22] O.Y. Gutierrez, G.A. Fuentes, C. Salcedo, T. Klimova, Stud. Surf. Sci. Catal. 162 (2006) 355.

[23] A. Wingen, N. Anastasievic, A. Hollnagel, D. Werner, F. Schuth, J. Catal. 193 (2000) 248.

[24] M.V. Landau, L. Titelman, L. Vradman, P. Wilson, Chem. Commun. (2003) 594.

[25] H.O. Zhu, J. Wang, C.Y. Zeng, D.Y. Zhao, Stud. Surf. Sci. Catal. 146 (2003) 661.

[26] D. Zhao, Q. Huo, J. Feng, B.F. Chmelka, G.D. Stucky, J. Am. Chem. Soc. 120 (1998) 6024.

[27] (a) S.-Y. Chen, L.-Y. Jang, S. Cheng, Chem. Mater. 16 (21) (2004) 4174; (b) G. Murali Dhar, S. Garg, G.M. Kumaran, K. Soni, V.V.D.N. Prasad, J.K. Gupta, Prepr. Pap. Am. Chem. Soc., Div. Pet. Chem. 51 (1 and 2) (2006).

[28] B.S. Parekh, S.W. Weller, J. Catal. 47 (1977) 100.

[29] K.S.P. Rao, H. Ramakrishna, G. Murali Dhar, J. Catal. 133 (1992) 146.

[30] M.V. Landau, L. Vradman, X. Wang, L. Titelman, Micropor. Mesopor. Mater. 78 (2005) 117.

[31] L. Vradman, M.V. Landau, D. Kantorovich, Y. Koltypin, A. Gedanken, Micropor. Mesopor. Mater. 79 (2005) 307.

[32] D.S. Kim, I.E. Wachs, K. Segawa, J. Catal. 149 (1994) 268.

[33] D.S. Kim, Y. Kurusu, I.E. Wachs, F.D. Hardcastle, K. Segawa, J. Catal. 120 (1989) 325.

[34] H. Shimada, T. Sato, Y. Yoshimura, A. Nishijima, J. Catal. 110 (1988) 275.

[35] G. Murali Dhar, F.E. Massoth, J. Shabtai, J. Catal. 85 (1984) 53.

[36] H. Topsoe, B.S. Clausen, F.E. Massoth, in: J.R. Anderson, M. Boudart (Eds.), Hydrotreating Catalysis Science and Technology, vol. 11, Springer, New York, 1996.